



## Accepted Article

**Title:** Metal-Thiobenzoato Complexes: Synthesis, Structure and Processing as Carbon Supported Nanoparticles

**Authors:** Daniel Vallejo-Sánchez, Garikoitz Beobide, Oscar Castillo, Monica Lanchas, Antonio Luque, Sonia Pérez-Yáñez, and Pascual Roman

This manuscript has been accepted after peer review and appears as an Accepted Article online prior to editing, proofing, and formal publication of the final Version of Record (VoR). This work is currently citable by using the Digital Object Identifier (DOI) given below. The VoR will be published online in Early View as soon as possible and may be different to this Accepted Article as a result of editing. Readers should obtain the VoR from the journal website shown below when it is published to ensure accuracy of information. The authors are responsible for the content of this Accepted Article.

**To be cited as:** *Eur. J. Inorg. Chem.* 10.1002/ejic.201701475

**Link to VoR:** <http://dx.doi.org/10.1002/ejic.201701475>

7DOI: 10.1002/ejic.201701475 (will be filled in by the editorial staff)

## Metal-Thiobenzoato Complexes: Synthesis, Structure and Processing as Carbon Supported Nanoparticles

Daniel Vallejo-Sánchez,<sup>[a]</sup> Garikoitz Beobide,<sup>\*[a]</sup> Oscar Castillo,<sup>\*[a]</sup> Mónica Lanchas,<sup>[a]</sup> Antonio Luque,<sup>[a]</sup> Sonia Pérez-Yáñez,<sup>[a, b]</sup> Pascual Román<sup>[a]</sup>

**Keywords:** thiobenzoato / thiocarboxylato / single-source precursors / carbon supported nanoparticles / dry thermolysis

Six new compounds of formula  $[M(\text{TBn})_2\text{L}]$  [TBn: thiobenzoato; M: Pd(II), Zn(II), Cd(II); L: 2,2'-bipyridine (bpy), 1,10-phenanthroline (phen), 1,2-di-(4-pyridil)-ethylene (bpe), neocuproine (neo), adenine (ade)] were obtained by the reaction of  $M(\text{CH}_3\text{COO})_2 \cdot 2\text{H}_2\text{O}$  with thiobenzoic acid and *N*-heterocyclic ligands. The use of chelating ligands and adenine led to monomeric compounds:  $[\text{Pd}(\text{TBn})_2(\text{bpy})]$  (PdBPY),  $[\text{Pd}(\text{TBn})_2(\text{phen})]$  (PdPHEN),  $[\text{Zn}(\text{TBn})_2(\text{neo})]$  (ZnNEO),  $[\text{Cd}(\text{TBn})_2(\text{neo})]$  (CdNEO), and  $[\text{Cd}(\text{TBn})_2(\text{ade})(\text{CH}_3\text{OH})]$  (CdADE). In these compounds the metal is bonded to sulfur atoms of two Tbn anions while the remaining coordination positions are completed by the donor atoms of the ancillary ligands. The bridging capability of the bpe ligand gave rise to the polymeric  $[\text{Cd}(\text{TBn})_2(\mu\text{-bpe})]_n$  (CdBPE) compound.

The presence of direct sulfur-metal bonds and carbon rich co-ligands enabled these complexes to yield by means of a dry thermolysis process a set of metallic and metal sulfide nanoparticles embedded into a carbonaceous support. The process to produce the latter materials consisted in an aerobic thermolysis using moderate temperatures (300–500°C) and short exposure times (minute scale). The analysis of the XRD patterns and SEM/TEM images reveal that the carbonaceous matrix hosts well dispersed nanocrystallites. The influence of the M(II) atom, ancillary ligand and thermal treatment parameters on the crystalline phase, size and purity of the resulting carbon supported nanoparticles is discussed.

- [a] Departamento de Química Inorgánica, Facultad de Ciencia y Tecnología, Universidad del País Vasco (UPV/EHU), Apartado 644, E-48080 Bilbao, Spain  
 Fax: 34-94601-3500  
 E-mail: garikoitz.beobide@ehu.eus, oscar.castillo@ehu.eus  
<https://www.ehu.eus/en/web/dqi/>
- [b] Departamento de Química Inorgánica, Facultad de Farmacia, Universidad del País Vasco (UPV/EHU), E-01006 Vitoria-Gasteiz, Spain

### Introduction

Thiocarboxylato ligands provide a valuable tool to design and synthesise metal-complexes as the presence of both soft sulfur and hard oxygen donor sites implies not only the ability to bind metals of rather different nature,<sup>[1]</sup> but it also endorses appealing electronic properties such as luminescence and conductivity.<sup>[2]</sup> Apart from that, complexes of chalcogenide have been studied as precursors for the deposition of II/VI type semiconductor nanoparticles through single-source precursor routes,<sup>[3]</sup> which makes this kind of coordination compounds of particular interest due to the increasing demand of quantum dots (QDs) for technological applications.<sup>[4]</sup> Precisely, the single-source precursor routes employ sulfur containing coordination compounds as starting material since metal-chalcogenide bonds are already present in the structure. In this approach, the metal-organic precursor is dispersed in a coordinating solvent (usually amines or amides) and injected into a hot solution containing a surfactant in order to stabilize the chalcogenide particles and to limit their growth. Thus, nanoparticles (NPs) with narrow size distributions are achievable. More recently, an alternative procedure called solventless thermolysis have been the focus of several research

works,<sup>[5]</sup> as it allows to prepare nanostructures by using solely metal-organic precursors. In comparison to solvent assisted single-source precursor route, dry thermolysis implies lower costs as diminishes the use of toxic and environmentally unfriendly organic solvents and hardly extractable surfactants. In this solventless approach, during the heating process the ligands passivate the surface of the particle limiting its growth, and as consequence, determine its size. The nature of the ligand influences also on the final phase and crystallinity of the achieved metal chalcogenide.<sup>[6]</sup> In general, during the thermolysis of the precursor, moderate temperatures are used to prevent the sintering of the NPs, but it also implies a generally quite high percentage of carbon impurities because of the lack of sufficient energy to complete the elimination of the ligands.<sup>[7]</sup>

Although in a first instance the non-volatilized carbonaceous part could be considered a disadvantage, numerous studies prove that heterostructures based on semiconducting nanoparticles embedded in carbon materials show promising features for its implementation in batteries, electrocatalysis and photocatalysis.<sup>[8]</sup> In fact, the dispersion of metal nanoparticles on a carbon matrix is a common practice in industry since this class of hybrid materials are widely employed as electrochemical electrodes for fuel cell<sup>[9]</sup> and battery applications,<sup>[10]</sup> as well as heterogeneous catalyst for organic synthesis,<sup>[11]</sup> hydrodesulfurization,<sup>[12]</sup> wastewater treatment,<sup>[13]</sup> etc. Furthermore, the carbon matrix prevents the agglomeration and sintering of the nanoparticles and in the same way it serves as continuous, porous and conductive support. Conventional methods for the preparation of heterogeneous catalysts focus on impregnation or dip-coating techniques that require long optimization times to achieve reproducible and

homogeneous results.<sup>[14]</sup> The controlled decomposition of metal-organic precursors in solid state opens a novel synthetic single-stage route for the production of carbon-based nanocomposites implying benefits related to solvent dispensal, technical simplicity, and lower manufacturing cost.

In a previous work<sup>[15]</sup> we demonstrated that thiocarboxylato complexes can be employed as single-source precursors for the synthesis of zinc sulfide nanoparticles. It was concluded that dry thermolysis, under aerobic conditions, of thioacetato complexes favoured the formation of highly pure sulfides. In this work we are focused on replacing the thioacetato ligand by the more stable thiobenzoato ligand in combination with *N*-heterocycle ligands of different C/N ratio and aromaticity degree to provide a carbonaceous matrix for the resulting nanoparticles. In particular, six new M<sup>II</sup> (Pd, Cd, and Zn) thiobenzoate compounds containing *N*-donor ligands (phen, neo, bpy, bpe and ade) were prepared and structurally characterized, after which they were subjected to dry thermolysis under aerobic conditions and moderate temperatures to provide Pd/C, ZnS/C and CdS/C composites.

## Results and Discussion

This section describes first the crystal structures of the metal-organic precursors, as these data will support the discussion regarding the formation of carbonaceous composites of metal and metal sulfide nanoparticles (M/C and MS/C, respectively). Prior to the dry thermolysis experiments, a sub-section devoted to preliminary thermogravimetric analyses is presented in which decomposition mechanism and optimum treatment temperature ranges will be set. Thereafter, results on the dry thermolysis experiments are thoroughly discussed, detailing the microstructures and particle sizes obtained in each case, to end up with the influence of the thermal treatment parameters.

**Crystal structure of precursors.** At first glance, the coordination sphere of these complexes (Figures 1 and 2) involves two sulfur bonded thiobenzoate ligands and the remaining coordination positions are occupied by two nitrogen donor atoms from a chelating *N,N'*-heterocyclic ligand in compounds PdBPY, PdPHEN, ZnNEO and CdNEO and from two *N,N'*-pillared bridging ligands in compound CdBPE. In the case of CdADE, apart from the two S atoms, the coordination sphere is completed by a nitrogen atom from an adenine molecule and the oxygen atom of a methanol molecule. At deeper insight, coordination sphere and corresponding polyhedron can be affected by the semicoordination of thiocarboxylate O atoms which is dependent of the metal type and size as well as the bulkiness of the co-ligands of each compound. As expected from its electronic configuration, Pd<sup>II</sup> (d<sup>8</sup>) does not present such semicoordination (Pd...O: 3.32–3.39 Å; distances larger than the sum of the van der Waals radii) and it sets in all cases a square planar coordination geometry [S(sp)=0.70–0.81] (Table 1). On the contrary, the semicoordination of O atoms in Zn<sup>II</sup> and Cd<sup>II</sup> (d<sup>10</sup>) complexes leads to coordination numbers that

range from 4 to 6. Initially, ruling out the semicoordination of oxygen atoms, the coordination polyhedron (MN<sub>2</sub>S<sub>2</sub>) of ZnNEO, CdBPE, CdNEO and CdADE can be described as a distorted tetrahedron. The small ionic radius of Zn<sup>II</sup> imposes great steric hindrances that implies long Zn...O contacts (3.06 Å) and results into a coordination environment notably closer to the ideal tetrahedral geometry. On the other hand, the bigger Cd<sup>II</sup> size allows to set shorter Cd...O contacts (2.55–2.85 Å) and it leads to small deviation respect to polyhedrons of greater coordination numbers.

Table 1. Continuous shape measures (CShM) calculation results.<sup>[16]</sup>

Compound	Geometries <sup>[a]</sup>					
	C.N. = 4		C.N. = 5		C.N. = 6	
	SP	T	TBPY	SPY	OC	TPR
<i>PdBPY</i>	0.70	30.73	—	—	—	—
<i>PdPHEN</i>	0.81	28.56	—	—	—	—
<i>ZnNEO</i>	29.12	2.80	8.05	8.09	25.62	13.78
<i>CdBPE</i>	26.14	2.67	2.86	7.32	6.61	11.26
<i>CdNEO</i>	29.12	5.46	3.41	6.27	8.40	12.10
<i>CdADE</i>	28.23	2.06	3.29	3.89	11.78	4.53

[a] SP: square-planar, T: tetrahedron, TBPY: trigonal bipyramid, SPY: square pyramid, OC: octahedron, TPR: trigonal prism.

All compounds, except CdBPE, consist of discrete monomeric entities in which the supramolecular assembly is strongly determined by the interactions occurring between TBn and the *N*-donor co-ligand, as described below. Bpy and phen ligands in compounds PdBPY and PdPHEN are able to link complex entities through T-shaped aromatic interactions and weak C–H...O and C–H...S hydrogen bonds. On the contrary, the more extended neo ligand in compound ZnNEO establishes  $\pi$ - $\pi$  parallel stacking interactions that assisted by C–H...O hydrogen bonds assemble the monomeric entities into 1D supramolecular chains. The neo ligand in compound CdNEO, establishes again  $\pi$ - $\pi$  parallel stacking interactions between them to arrange monomeric entities into supramolecular dimers that are held together by means of T-shaped aromatic interactions and weak C–H...O and C–H...S hydrogen bonds. The presence of the bridging bpe ligand in compound CdBPE, affords a zig-zag 1D polymeric complex entity with Cd...Cd distances of 14.057 and 13.851 Å. These chains are held together by means of T-shaped aromatic interactions among the benzene aromatic rings and weak C–H...O and C–H...S hydrogen bonds. In compound CdADE, the adenine molecule is coordinated to the cadmium atom through its N7 donor position. This coordination mode is reinforced by an additional intramolecular hydrogen bond between the N6–H amino group and the oxygen atom of the coordinated methanol molecule. Further details on the crystal structures, including packing views and bond distances, are gathered in the supporting information.

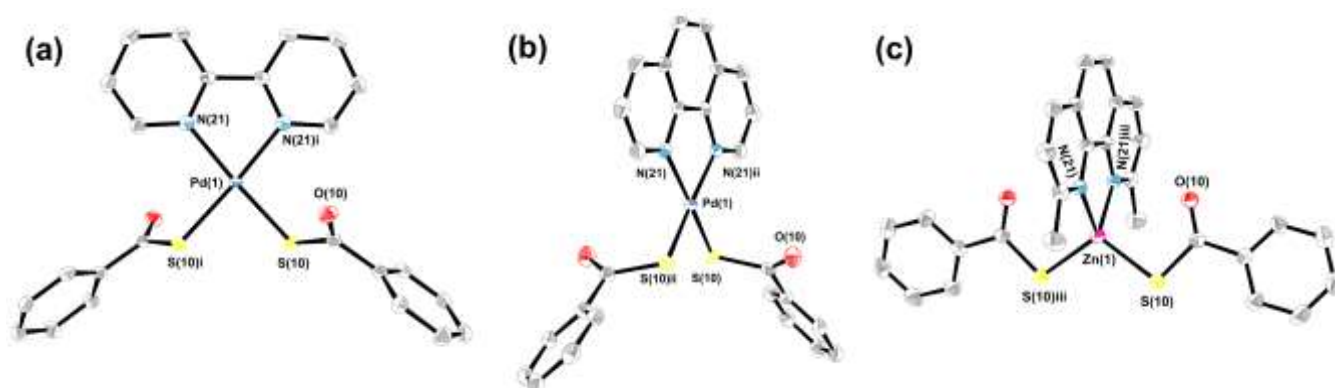


Figure 1. ORTEP diagrams of compounds (a) PdBPY, (b) PdPHEN, and (c) ZnNEO showing the labelling scheme. Hydrogen atoms are omitted for clarity. Symmetry codes: (i)  $-x+1, y, -z+1/2$ ; (ii)  $-x+3/2, y, -z+1$ ; (iii)  $-x+1, y, -z+3/2$ .

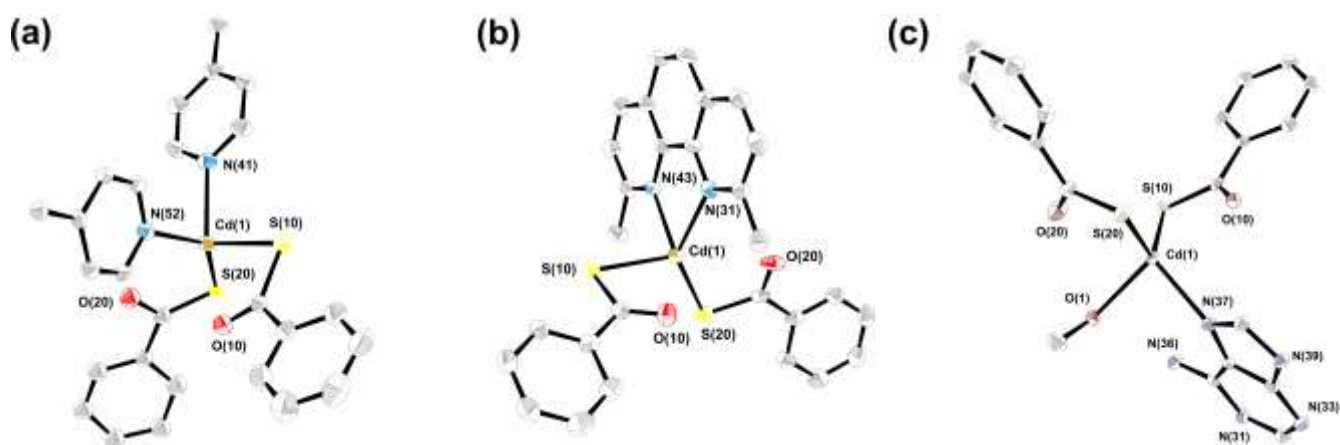


Figure 2. ORTEP diagrams of compounds (a) CdBPE, (b) CdNEO, and (c) CdADE showing the labelling scheme. Hydrogen atoms are omitted for clarity.

**Decomposition mechanism and optimum treatment temperature.** The evaluation of synthesized compounds as single-source precursors for carbon supported nanomaterials was initially checked by thermogravimetric measurements in order to define an optimum range to afford desired products. The thermal degradation under synthetic air atmosphere shows (Figure 3a) that all compounds start their decomposition at relatively low temperatures (PdBPY: 198°C; PdPHEN: 230°C; ZnNEO: 239°C; CdBPE: 220°C; CdNEO: 237°C; CdADE: 151°C). Apparently, the decomposition temperatures are more dependent on the nature of the co-ligands than on the type of the metal centers. In fact, compounds containing a chelating ligand with three fused aromatic hexagonal rings (phen and neo), provide thermally more robust products (230–240°C) whereas the remaining compounds are notoriously less stable. The analysis of DTA curves (Figure 3b) indicates the occurrence of an endothermic event possibly related to a pyrolytic partial fragmentation of the ligands. After this first mass loss all compounds achieve a more or less stable plateau that corresponds to a variable mixture of PdSO<sub>4</sub> or M<sup>II</sup>S (M<sup>II</sup>: Zn, Cd) nanoparticles and amorphous carbon, as confirmed by PXRD and microanalysis of these intermediates (see Table S3.1 in the supporting information). Precursors provided with non-fused pyridine ligands such as bpe and bpy generate samples with low carbon content (2–4 %) as the fragments formed during the thermolysis (*i.e.* pyridine, methylamine, H<sub>2</sub>O, NH<sub>3</sub>) are more volatile in nature.<sup>[17]</sup> In

precursors PdBPY and PdPHEN, the previously formed PdSO<sub>4</sub> decomposes around 330–350 °C to form elemental palladium.

At greater temperatures, between 295 and 485°C, there is a second weight loss consisting of an overlapped set of exothermic stages related to the oxidation of the carbonaceous phase. Amorphous carbon typically burns at temperatures ranging from 550 to 610°C under aerobic conditions.<sup>[18]</sup> Nevertheless, in PdBPY and PdPHEN a substantial lowering in the combustion temperature is noticed implying a decrease of *ca.* 300°C respect to the typical onset temperature. This fact is explained by the catalytic activity of palladium prompting the oxidation of soot.<sup>[19]</sup> In group 12 transition metal precursors, the metal sulfide is further oxidized to give ZnO (JPDS: 01-075-0576; *P6<sub>3</sub>mc*) in the case of ZnNEO or a mixture of CdO (JPDS: 00-001-1049; *Fm-3m*) and cadmium oxysulfate (JPDS: 00-032-0140; *Cm2a*) for CdBPE, CdNEO and CdADE. In PdBPY and PdPHEN, at this temperature range, the previously formed elemental palladium undergoes a passivation with the consequent formation of a thin layer of PdO (JCPDS: 01-075-0584; *P-4n2*). Additional thermoanalytic data are available in the supporting information.

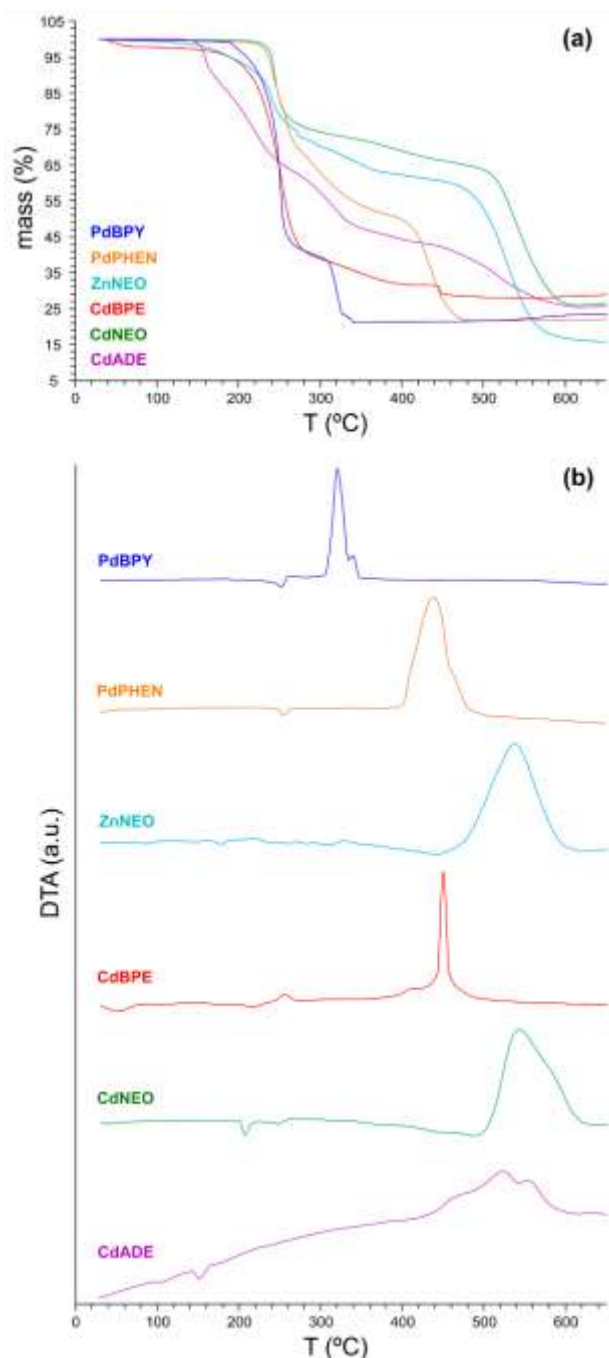


Figure 3. (a) Thermogravimetric analysis of metal(II)-thiobenzoate compounds under synthetic air atmosphere and (b) their corresponding DTA curves.

Table 2. Main characteristics of the dry thermolysis products obtained under aerobic conditions.

Precursor	T (°C)	Products (JPDS Card) [a]	D <sub>XRD</sub> (nm) [b]	D <sub>TEM</sub> (nm) [c]	C.V. (%) [d]	C (% wt) [e]
PdBPY	345	Pd (01-087-0638)	60	3±1 / 119±52	33.3 / 43.7	1.6
PdPHEN	480	Pd (01-087-0638) PdO (01-075-0584)	70	21±6 / 78±26	28.6 / 33.3	38.4
ZnNEO	400	w-ZnS (00-036-1450)	9	8±2	25.0	41.8
CdBPE	400	c-CdS (00-042-1411) w-CdS (01-077-2306)	13 (blende) 8 (wurtzite)	28±8	28.6	3.9
CdNEO	480	w-CdS (01-077-2306)	19 (wurtzite)	35±9	25.7	42.7
CdADE	400	c-CdS (00-042-1411)	11 (blende)	16±4	25.0	22.2

[a] JPDS card number. [b] Mean particle size estimated from Debye-Scherrer equation. Diffraction peaks chosen for each crystalline phase: (111) for Pd, (110) for w-ZnS, (110) for w-CdS and (200) for c-CdS. [c] Mean particle size along with its standard deviation calculated from the statistical analysis of TEM images. [d] C.V.: coefficient of variation. [e] Carbon mass percentage calculated by thermogravimetry.

**Dry thermolysis experiments.** The aforementioned results indicate that by controlling the thermal decomposition process it is possible to access metal and metal sulfides even under aerobic conditions. It deserves to note that, as far as we are concerned, all the dry thermolysis processes reported up to date, except our previous work,<sup>[15]</sup> make use of an inert atmosphere in order to yield the corresponding metal chalcogenide. Taking into account the results of the thermogravimetric analyses, precursor powders were introduced for 15 minutes in a tubular oven open to air and preheated to a temperature at which intermediate sulfides or palladium metal are expected to be formed (see Table 2).

The X-ray diffraction profiles taken on thermolysis products prove their crystalline nature (Figure 4) and confirm the achievement of the pursued phase. In the residues of compounds PdBPY and PdPHEN the cubic phase of elemental palladium is found. Additionally, in compound PdPHEN a small peak corresponding to the plane (110) of tetragonal PdO is glimpsed. The resulting ZnS obtained from compound ZnNEO corresponds to the wurtzite phase. This polymorph is metastable at standard conditions in bulk state (the transformation from blende to wurtzite occurs at 1020 °C)<sup>[20]</sup> and it is more interesting than the blende cubic phase in terms of optoelectronic properties.<sup>[21]</sup> CdS obtained from compound CdBPE corresponds to a mixture of wurtzite and blende polymorphs, but CdNEO and CdADE precursors render the pure CdS wurtzite and blende phases, respectively. Thus, it can be concluded that the correct choice of the N-donor co-ligand allows stabilizing a specific crystalline phase.

The amount of carbon accompanying nanoparticles, ranging from 2 to 43 %wt, depends on the starting material, being notorious the presence of a greater percentage of carbon in compounds containing molecules with fused aromatic rings as ancillary ligand (PdPHEN, ZnNEO, CdADE and CdNEO).

The average crystallite size of the as-synthesized nanoparticles was estimated from Debye-Scherrer<sup>[22]</sup> equation (Table 2). The great widening of diffraction peaks observed in ZnS and CdS samples reveals the nanometric nature of the crystalline domains for which size estimate ranges from 8 to 19 nm. In contrast, full widths at half maximum (FWHM) of the measured signals for metal palladium samples are markedly thinner, and lead to crystallite size of 60–70 nm. Note that particle size obtained from XRD analyses corresponds to the statistic of the bulk sample, and the contribution of the smallest particles is masked. This fact will be further discussed in TEM (transmission electron microscopy) analyses.

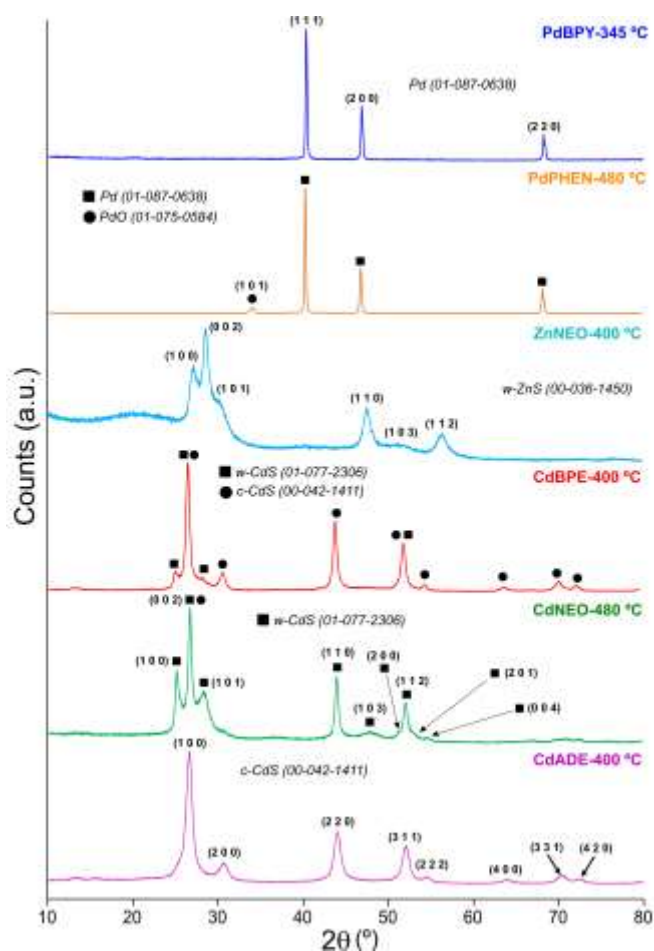


Figure 4. X-ray diffraction patterns of dry thermolysis products obtained under aerobic conditions at 345–480°C for 15 minutes.

SEM images were performed over combustion samples in order to inquire into their microstructural characteristics (Figure 5). Thermolysis products of PdBPY and PdPHEN consist of compact microsized aggregates with smooth surfaces. At high magnifications, the nanoparticles embedded in the carbon matrix are hardly discerned, despite they will become clear in below described TEM analysis. In the case of ZnNEO, the obtained product shows greater compositional heterogeneities at nanometric scale since ZnS nanoparticles tend to aggregate forming clusters of approximately 1–3 micron. Thermolysis of CdBPE generates an agglomerated granular nanotexture indicative of the presence of partially sintered nanocrystallites. CdS/C nanocomposite prepared from compound CdNEO presents a higher surface rugosity in comparison to the product of ZnNEO (despite both precursors contain neocuproine ligand). The dispersed CdS nanoparticles exhibit a well-defined spherical shape and are better distributed along the carbon matrix at nanoscale. Like carbon-rich precursors (PdPHEN, ZnNEO and CdNEO), compound CdADE degrades creating completely compact and glassy surfaces. However, the compositional arrangement of the material is just the reverse: carbon is grouped forming microparticles and these are surrounded by a matrix composed of CdS nanoparticles linked to each other through a thin carbon coating (Figure 6a-d). This unexpected phenomenon will be discussed later when analyzing the TEM images of samples.

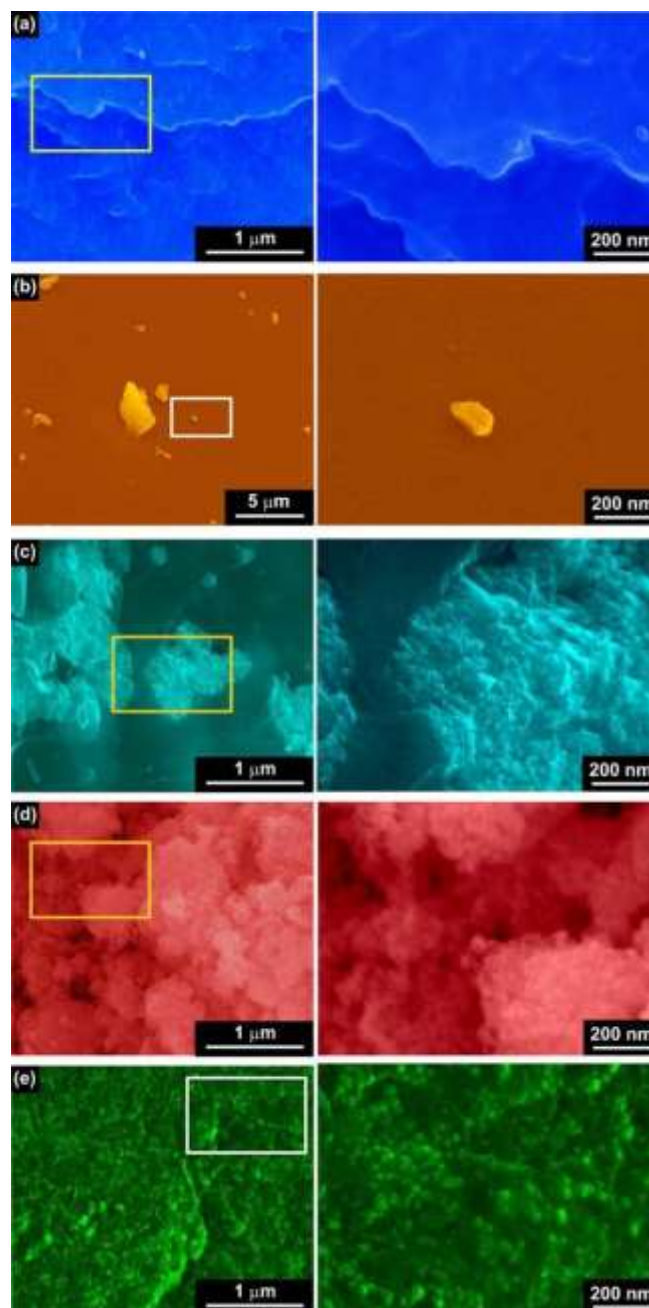


Figure 5. SEM images (10 kX of magnification on the left and 100 kX rightwards) of decomposition products synthesised from (a) PdBPY, (b) PdPHEN, (c) ZnNEO, (d) CdBPE and (e) CdNEO after having been subjected to 345–480°C for 15 minutes.

TEM was employed to get a better insight into the generated nanocomposites (Figure 7). Transmission micrographs confirm the existence of nanoparticles dispersed into an amorphous carbonaceous matrix. Data on statistical particle size analysis of the TEM images are provided in Table 2. Accordingly, elemental palladium nanoparticles display a bimodal size distribution in which fine particles (3–21 nm) (Figure 7a-b) and coarse particles (>40 nm) (Figure S5.8) can be distinguished. With regard to particle morphology, spherical particles and low aspect ratio nanorods are obtained for PdBPY and PdPHEN, respectively. This clue suggests that the heterocyclic co-ligand plays a key role in both size and morphology of the resulting Pd nanoparticles.

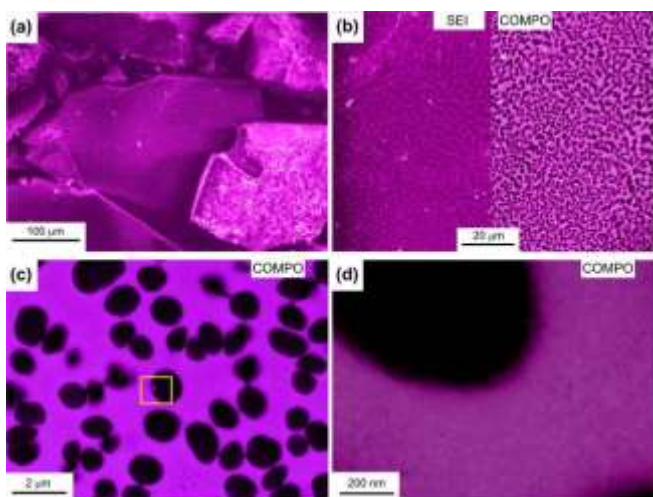


Figure 6. SEM images at different magnifications obtained for thermolysis product of compound CdADE (400°C for 15 min).

On the contrary, the sizes found for metal sulfide nanoparticles show smaller polydispersion (coefficients of variation less than 29 %) and generally, smaller than 60 nm (Figure 8). The resulting sizes are comparable to those obtained by wet routes in which surfactants are employed to control particle growth kinetics.<sup>[23]</sup> All

of them have monomodal curves except CdS nanoparticles prepared from CdNEO which describe a bimodal behavior with maxima around 25–30 nm and 35–40 nm. The effect of the metal center on particle size also becomes evident by observing the size distributions of sulfide obtained from ZnNEO and CdNEO; ZnS obtained from ZnNEO is composed of nanoparticles lower than 15 nm whereas all CdS nanoparticles generated from CdNEO exceed this limit.

TEM images taken on thermolysis product of CdADE will serve to enlighten about the mechanism of formation of the aforementioned micrometric carbon clusters (Figure 6). During dry thermolysis, the first nucleation points appear at the surface of the precursor grains and they grow by incorporating the further cadmium and sulfur atoms that diffuse from inner core of the grain. As semiconducting nanoparticles are formed, they tend to diffuse towards grain boundaries and accumulate therein creating a species of halos for greater carbonaceous agglomerates (Figure S5.9) but a more homogeneous dispersion is obtained for smaller ones. When the grain size is relatively small ( $< 1 \mu\text{m}$ ) this phenomenon is not observable because nanoparticles do not have enough space to move and well dispersed agglomerates are generated.

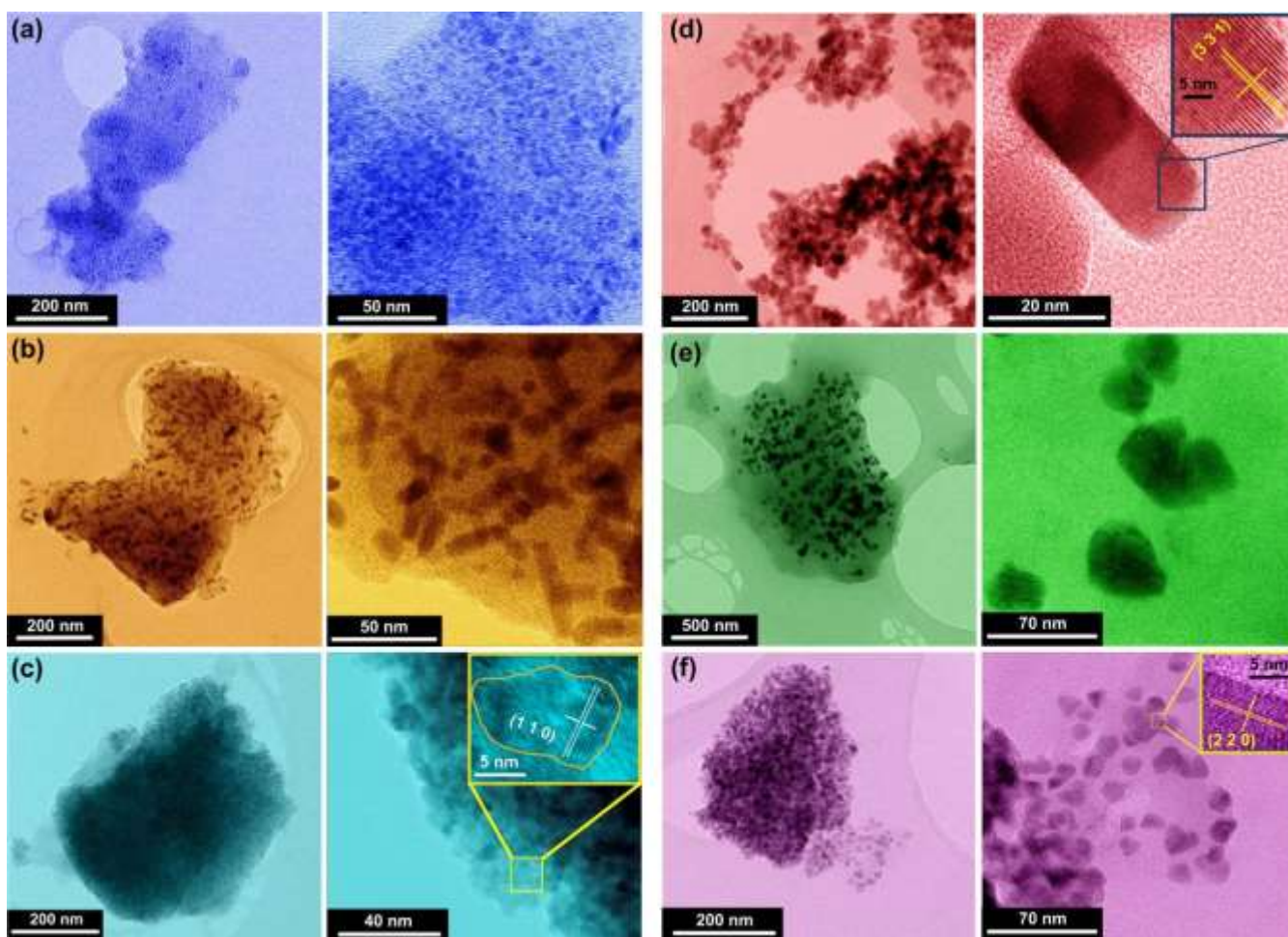


Figure 7. TEM images of thermolysis products: (a) PdBPY, (b) PdPHEN, (c) ZnNEO, (d) CdBPE, (e) CdNEO and (f) CdADE.

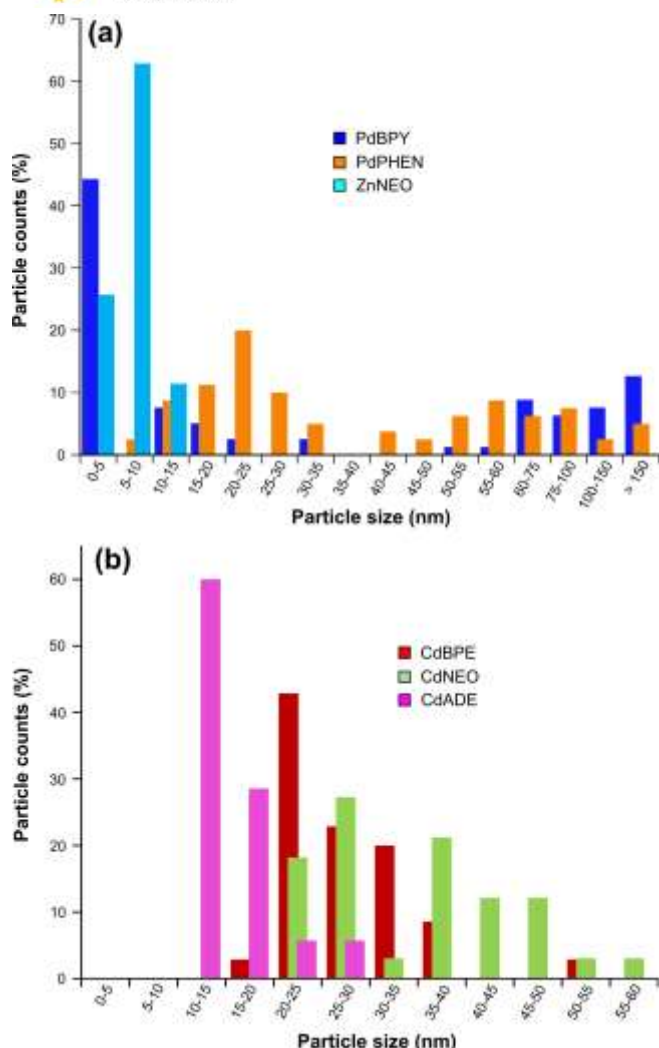


Figure 8. Particle size histograms estimated from TEM images acquired for different decomposition products.

On the other hand, decomposition products show a low degree of agglomeration of nanoparticles within the carbon matrix, being noticeable the individual morphology of themselves along the solid. In MS/C samples, it has even been possible to identify certain crystallographic orientations (Figure S5.10) in contrast to Pd/C nanocomposites. The interplanar distances measured match those expected for each decomposition product: 0.1977 nm for sample ZnNEO which corresponds to the plane (110) of ZnS wurtzite phase, 0.1743 nm for sample CdBPE which coincides with the plane (331) of the CdS cubic phase, 0.2474 nm for sample CdNEO which adjusts to (102) reflection of CdS wurtzite phase and 0.2086 nm for sample CdADE which is consistent with (220) index of CdS cubic polymorph. Each decomposition product has been subjected to qualitative compositional measurements using EDX analysis (Figure S5.11). In zones with lower contrast (*i.e.* matrix rich zone) the carbon ratio is substantially higher, being this increment more abrupt in carbon rich products obtained from PdPHEN, ZnNEO, CdNEO and CdADE. In the case of Pd/C nanocomposites, spectra realized over these brighter areas also show an additional peak corresponding to S element with a Pd/S ratio close to the unity.

Thus, the carbonaceous matrix in palladium products contains also amorphous phase of sulfide or palladium sulfate which has not yet been reduced to metal (note, that according to thermogravimetric analysis PdSO<sub>4</sub> precedes to the formation of elemental Pd). This sulfur impurities together with the small particle size in PdBPY and high carbon content in PdPHEN seems to hinder the recognition of crystallographic planes.

**Influence of thermal treatment parameters.** In order to understand the degree of influence of the main thermolysis variables on the particle size, crystallinity and the final carbon content of the product, different thermogravimetric tests were performed on the precursor PdBPY. Despite particle size polydispersion found in elemental Pd samples, Debye-Scherrer analysis and TEM images allow to monitor how coarse and fine particles evolve, respectively. When fixing the onset temperature at 345°C, TEM images (Figure 9) show how finest particles tend to grow progressively from 3–5 nm at five minutes of treatment time to 80–200 nm after sixty minutes. Considering that the carbon matrix prevents the particle sintering, its elimination as the exposure time increases, prompts the nuclei growth by following Ostwald's maturation but also their aggregation into bigger sized cumuli (500–1000 nm). Accordingly, the flattening of PXRD background (Figure S4.2) as the treatment time increases is also consistent with the decrease of the amorphous carbon amount. Similarly carbonaceous matrix is also reduced when increasing the onset temperature (at fixed exposure time and heating rate; Figure S4.3) and lowering heating rate (at fixed exposure time and onset temperature; Figure S4.4). Again, Debye-Scherrer analysis (Table 3) does not allow to follow the evolution of finest particles, but it indicates that after fifteen minutes the sintering of small particles into coarse crystallites reaches a limit close to 60 nm. Regarding influence of thermal treatment parameters on the formation of metal sulfides, ZnNEO and CdNEO have been selected as representative cases. Unlike Pd particles, the size of ZnS and CdS particles is not affected by the exposure temperature and time within the analysed range (400–480°C; < 60 min).

Table 3. Debye-Scherrer expression based crystallite size analysis of cadmium and zinc based compounds.

Precursor	T (°C) [a]	r <sub>H</sub> (°C·min <sup>-1</sup> ) [b]	t (min)	(hkl)	D <sub>v</sub> (nm)
PdBPY	345	5	5	(111)	41
	345	5	15	(111)	60
	345	5	30	(111)	66
	345	5	60	(111)	57
	345	15	5	(111)	32
	345	15	15	(111)	69
	345	30	5	(111)	[c]
	360	15	5	(111)	67
ZnNEO	400	[d]	15	(110)-w	9
	480	[d]	15	(110)-w	9
	480	[d]	60	(110)-w	8
CdNEO	400	[d]	15	(110)-w	15
	480	[d]	15	(110)-w	19
	480	[d]	60	(110)-w	17

[a] Combustion temperature. [b] Heating rate. [c] The crystallite size could not be estimated due to the large background level exhibited that partially obscures the diffraction peaks. [d] The precursor was introduced into a preheated oven.

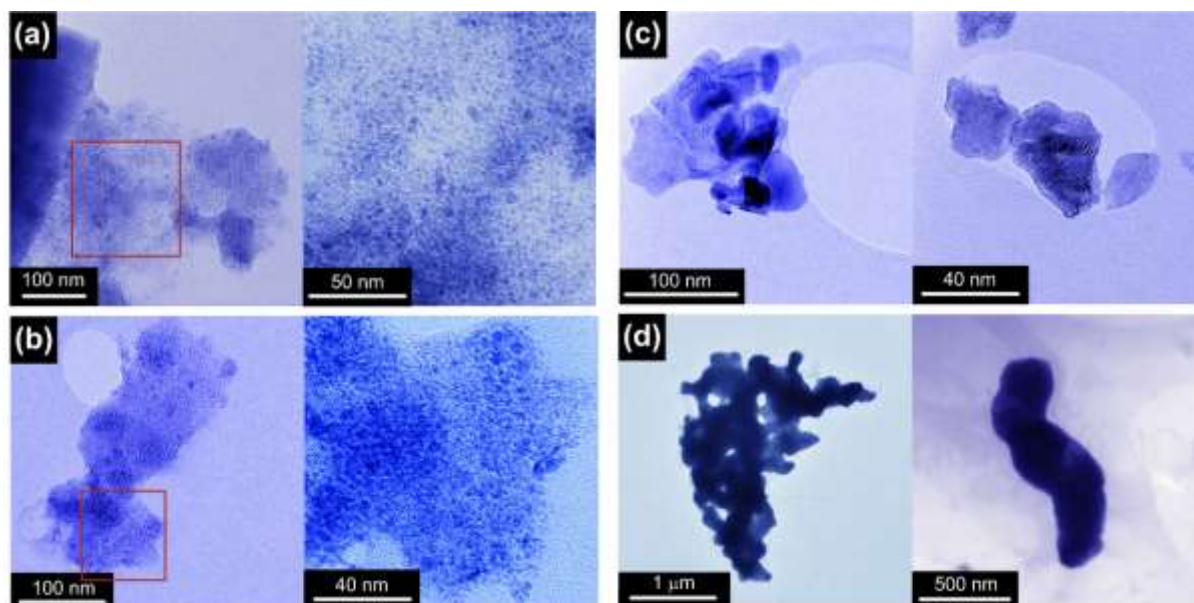


Figure 9. TEM images of the products obtained from compound PdBPY at different combustion times: (a) 5 min, (b) 15 min, (c) 30 min, and (b) 60 min.

## Conclusions

We have obtained six different air-stable metal-thiobenzoato compounds (M: Pd, Zn, Cd) containing *N*-heterocycles (bpy, phen, neo, bpe and ade) to complete the coordination sphere of the metal(II) atom. The presence of direct metal-sulfur bonds is a key factor to use these compounds as single-source precursors for the synthesis of nanometric chalcogenide particles. Despite thiocarboxylate based compounds are characterized by experiencing complete decompositions at relatively low temperatures,<sup>[24]</sup> the use of ligands containing aromatic rings make feasible to afford through a mild thermolysis treatment in air atmosphere carbon supported metal and metal sulfide nanocrystallites. The nature of the starting metal-thiobenzoato precursor seems to exert a crucial influence on the final blende or wurtzite crystalline phase of the resulting metal(II) sulfide nanoparticles, as neocuproine based compounds with  $\pi$ -extended systems give rise to wurtzite phase, whereas less  $\pi$ -extended adenine and 1,2-di-(4-pyridil)-ethylene provide blende phase and mixture of both polymorphic phases, respectively. The carbon content in each sample is also strongly influenced by the nature of the co-ligand. Phen, neo and ade form non-volatile byproducts during pyrolysis resulting in carbonaceous matrices, whereas less fused ligands such as bpy and bpe practically generate pure samples.

Zn(II) and Cd(II) metal-organic precursors render metal(II) sulfide nanoparticles with a fine size distributions and mean size values ranging from 8 to 19 nm. On the contrary, Pd(II) complexes lead to metal nanoparticles with a significant polydispersion, where fine particles (3–20 nm) and coarser ones (< 40 nm) can be distinguished. Accordingly, the analysis of thermal treatment parameters shows that the formation of Pd nanoparticles is highly sensitive to exposure time, heating rates and onset temperature, in such a way that sintering and nuclei growth can be notably affected. On the other hand, size of the formed metal(II) sulfide nanoparticles is not notably influenced by aforementioned parameters, which makes them more reliable product for a hypothetical upscaling. Thus, the single-step method for obtaining

nanostructures does not require expensive equipment and production times are brief. Furthermore, the possibility of working under aerobic conditions reduces costs substantially. All these reasons make dry thermolysis an interesting synthetic method in order to satisfy the industrial demand of this class of materials.

## Experimental Section

**General information.** Commercially available zinc acetate dihydrate ( $\text{Zn}(\text{OAc})_2 \cdot 2\text{H}_2\text{O}$ ), cadmium acetate dihydrate ( $\text{Cd}(\text{OAc})_2 \cdot 2\text{H}_2\text{O}$ ), palladium acetate ( $\text{Pd}(\text{OAc})_2$ ), thiobenzoic acid (HTBn), 2,2'-bipyridine (bpy), 1,10-phenanthroline (phen), neocuproine (neo), 1,2-di-(4-pyridil)-ethylene (bpe), adenine (ade) and all the solvents were of analytical grade and they were used without further purification. The new compounds are stable in air at room temperature. Data on the solubility of the compounds in common solvents is provided in the supporting information. The yields calculated are based on metal salt.

**[Pd(TBn)<sub>2</sub>(bpy)]** (PdBPY): 2.5 mmol (0.561 g) of  $\text{Pd}(\text{OAc})_2$  were dissolved in 45 mL of *N,N'*-dimethylformamide (DMF). In another beaker, 2.5 mmol of bpy (0.390 g) and 5 mmol (430  $\mu\text{L}$ ) of HTBn were dissolved in 5 mL of DMF. The resulting solution was added over the solution containing the metal salt while it was subjected to magnetic stirring. In few seconds the dark reddish solution became opaque by the appearance of a yellowish polycrystalline powder of PdBPY. One hour later the obtained product was filtered and then washed several times with methanol (MeOH) to finally be dried at room temperature for one day. The filtrate was left undisturbed at room temperature to obtain yellow single crystals of PdBPY suitable for X-ray diffraction analysis. Yield (based on metal salt): 0.8993 g (67%). Main IR features of compound PdBPY ( $\tilde{\nu}(\text{cm}^{-1})$ ): 3163(vw), 3104(w), 3093(vw), 3078(w), 3058(w), 3029(vw), 2995(vw), 1671(w), 1609(vs), 1595(vs), 1573(s), 1491(w), 1483(w), 1464(w), 1441(s), 1415(w), 1387(vw), 1318(w), 1313(w), 1303(m), 1290(w), 1277(vw), 1263(vw), 1257(vw), 1245(w), 1201(s), 1175(m), 1119(vw), 1104(w), 1096(vw), 1080(w), 1066(w), 1044(vw), 1030(w), 1020(w), 1005(vw), 992(vw), 972(vw), 931(m), 907(s), 846(vw), 800(vw), 775(m), 763(s), 725(m), 702(m), 695(s), 660(m). Anal. Found (%): C, 53.79; H, 3.45; N, 5.42; Pd, 19.55; S, 11.88. Calc. for  $\text{C}_{24}\text{H}_{18}\text{N}_2\text{O}_2\text{PdS}_2$  (%): C, 53.68; H, 3.38; N, 5.22; Pd, 19.82; S, 11.94.

**[Pd(TBn)<sub>2</sub>(phen)]** (PdPHEN): The synthetic procedure was similar to that of PdBPY, except that phen (2.5 mmol, 0.450 g) was used instead of bpy. In this case ligands were added sequentially onto the solution containing the dissolved metal salt (first HTBn and then phen). The polycrystalline product of PdPHEN was washed with MeOH. The mother liquors were left undisturbed at room temperature to obtain yellow single crystals. Yield: 1.1503 g (82%). Main IR features of compound PdPHEN  $\bar{\nu}(\text{cm}^{-1})$ : 3158(vw), 3143(vw), 3067(w), 3024(w), 2992(w), 2926(vw), 2856(vw), 1674(m), 1608(vs), 1595(vs), 1570(vs), 1513(m), 1496(w), 1481(w), 1449(sh), 1444(m), 1421(s), 1413(w), 1403(w), 1387(w), 1338(m), 1318(w), 1309(w), 1290(w), 1253(vw), 1218(vw), 1193(s), 1167(s), 1143(w), 1106(m), 1093(w), 1076(w), 1056(vw), 1036(vw), 1024(vw), 1000(vw), 987(vw), 931(m), 908(vs), 875(w), 847(s), 813(vw), 797(vw), 776(s), 739(w), 723(vw), 718(s), 691(s).

Anal. Found (%): C, 55.58; H, 3.16; N, 5.04; Pd, 19.09; S, 11.37. Calc. for C<sub>26</sub>H<sub>18</sub>N<sub>2</sub>O<sub>2</sub>PdS<sub>2</sub> (%): C, 55.67; H, 3.23; N, 4.99; Pd, 18.97; S, 11.43.

**[Zn(TBn)<sub>2</sub>(neo)]** (ZnNEO): The procedure is similar to that of compound PdBPY. Zn(OAc)<sub>2</sub>·2H<sub>2</sub>O (2.5 mmol, 0.545 g) was used instead of Pd(OAc)<sub>2</sub> and bpy was replaced by neo (2.5 mmol, 0.520 g). The solvent selected for the reaction was MeOH. In few seconds the colorless solution became opaque by the appearance of a whitish polycrystalline powder of ZnNEO. One hour later the obtained product was filtered and then washed several times with methanol (MeOH) to finally be dried at room temperature for one day. The filtrate was left undisturbed at room temperature to obtain colourless single crystals. Yield: 1.2052 g (88 %). Main IR features of compound ZnNEO  $\bar{\nu}(\text{cm}^{-1})$ : 3065(w), 3022(w), 1619(w), 1596(vs), 1567(vs), 1500(m), 1481(w), 1441(m), 1426(w), 1375(w), 1337(vw), 1325(vw), 1299(w), 1245(vw), 1220(w), 1194(vs), 1164(s), 1151(sh), 1130(sh), 1098(vw), 1071(vw), 1054(vw), 1026(w), 1001(vw), 987(vw), 970(vw), 920(vs), 853(m), 843(w), 813(vw), 791(sh), 781(sh), 774(m), 729(w), 691(s), 683(m), 663(vw). Anal. Found (%): C, 61.45; H, 3.92; N, 5.08; S, 11.75; Zn, 11.94. Calc. for C<sub>28</sub>H<sub>22</sub>N<sub>2</sub>O<sub>2</sub>S<sub>2</sub>Zn (%): C, 61.37; H, 4.05; N, 5.11; S, 11.70; Zn, 11.93.

**[Cd(TBn)<sub>2</sub>(μ-bpe)]<sub>n</sub>** (CdBPE): The synthetic procedure was similar to that of ZnNEO, except that Cd(OAc)<sub>2</sub>·2H<sub>2</sub>O (2.5 mmol, 0.670 g) was used as metal source, bpe (2.5 mmol, 0.455 g) was used instead of neo and HTBn was added firstly onto metal solution. After one hour of reaction a yellowish powder of CdBPE was recovered. The filtrate was left undisturbed at room temperature to obtain yellow single crystals. Yield: 1.1239 g (79 %). Main IR features of compound CdBPE  $\bar{\nu}(\text{cm}^{-1})$ : 3068(vw), 3050(vw), 3024(vw), 1601(vs), 1555(s), 1537(s), 1501(m), 1483(w), 1445(w), 1426(s), 1351(w), 1304(w), 1259(vw), 1247(vw), 1204(vs), 1168(s), 1155(sh), 1115(vw), 1097(vw), 1068(m), 1019(w), 1011(m), 1001(w), 982(m), 961(w), 938(s), 923(s), 866(w), 845(sh), 833(s), 799(sh), 775(s), 742(vw), 721(vw), 689(vs), 675(sh), 652(w). Anal. Found (%): C, 54.92; H, 3.57; Cd, 19.70; N, 4.87; S, 11.21. Calc. for C<sub>26</sub>H<sub>20</sub>CdN<sub>2</sub>O<sub>2</sub>S<sub>2</sub> (%): C, 54.88; H, 3.54; Cd, 19.76; N, 4.92; S, 11.27.

**[Cd(TBn)<sub>2</sub>(neo)]** (CdNEO): The synthetic procedure was similar to that of CdBPE, except that neo (2.5 mmol, 0.520 g) was used instead of bpe. The polycrystalline product of CdNEO was washed with MeOH. The mother liquors were left undisturbed at room temperature to obtain pale-yellow single crystals. Yield: 1.3831 g (93 %). Main IR features of compound CdNEO  $\bar{\nu}(\text{cm}^{-1})$ : 3053(w), 3022(w), 2999(vw), 2966(vw), 2922(vw), 1616(w), 1590(m), 1539(s), 1502(s), 1441(m), 1410(w), 1376(w), 1364(w), 1305(w), 1291(w), 1251(vw), 1207(vs), 1172(m), 1152(m), 1118(sh), 1102(vw), 1075(w), 1025(w), 994(vw), 931(vs), 858(m), 844(w), 810(vw), 793(vw), 773(m), 728(w), 691(vs), 654(w). Anal. Found (%): C, 56.50; H, 3.62; Cd, 18.78; N, 4.80; S, 10.86. Calc. for C<sub>28</sub>H<sub>22</sub>CdN<sub>2</sub>O<sub>2</sub>S<sub>2</sub> (%): C, 56.52; H, 3.72; Cd, 18.89; N, 4.71; S, 10.79.

**[Cd(TBn)<sub>2</sub>(ade)]** (CdADE): 2.5 mmol (0.670 g) of Cd(OAc)<sub>2</sub>·2H<sub>2</sub>O was dissolved in 40 mL of MeOH and allowed to stir at room temperature. In

another beaker, 2.5 mmol (0.338 g) of ade and 5 mmol (430 μL) of HTBn were mixed in 8 mL of hot MeOH. Immediately, the mixture becomes clear and after one hour of stirring at room temperature the yellow solution is kept in a refrigerator at about 5 °C. Several days after CdADE appeared as colourless single-crystals mixed with a whitish polycrystalline powder. Yield: 0.7614 g (55 %). Main IR features of compound CdADE  $\bar{\nu}(\text{cm}^{-1})$ : 3240(m), 3154(m), 3053(s), 2963(m), 2814(m), 2714(w), 2668(w), 1678(vs), 1647(w), 1599(w), 1585(m), 1545(sh), 1524(s), 1512(s), 1445(s), 1427(m), 1414(m), 1337(m), 1308(w), 1230(sh), 1204(vs), 1167(s), 1119(w), 1101(w), 1076(w), 1059(sh), 1026(vw), 999(vw), 937(s), 916(s), 895(m), 843(w), 824(w), 775(m), 716(vw), 690(s), 656(w). Anal. Found (%): C, 43.33; H, 3.49; Cd, 20.31; N, 12.67; S, 11.62. Calc. for C<sub>20</sub>H<sub>19</sub>CdN<sub>5</sub>O<sub>3</sub>S<sub>2</sub> (%): C, 43.36; H, 3.46; Cd, 20.29; N, 12.64; S, 11.58.

**Physical measurements.** Elemental analyses (C, H, N, S) were performed on a Euro EA Elemental Analyzer, whereas the metal content was determined by inductively coupled plasma (ICP-AES) using a Horiba Yobin Yvon Activa spectrometer. Infrared spectra (ATR mode) were recorded at a resolution of 4 cm<sup>-1</sup> on a FTIR 8400S Shimadzu spectrophotometer for a total of 40 scans in the 4000–650 cm<sup>-1</sup> spectral region. Thermal analysis (TG/DTG/DTA) were carried out on a Mettler Toledo TGA/SDTA 851e thermal analyser employing a synthetic air (79% N<sub>2</sub>, 21% O<sub>2</sub>) flux of 150 cm<sup>3</sup>·min<sup>-1</sup> with heating rates of 5–30 °C·min<sup>-1</sup> and a sample size of about 10–25 mg per run. Combustions of precursors were performed under aerobic conditions using a Carbolite 3216 tubular furnace. The X-ray powder diffraction patterns (PXRD) were collected on a X-Pert PRO PAN analytical machine employing a Cu K $\alpha$  radiation source at a scanning rate of 0.026°·s<sup>-1</sup>. The average diameter of particles (D<sub>v</sub>) has been calculated from D<sub>v</sub> = (4/3)·L<sub>v</sub> expression. L<sub>v</sub> = K·λ/β·cosθ, where L<sub>v</sub> is the volume-weighted average crystallite size measured in a direction perpendicular to surface of the specimen, λ is the average wavelength, in nanometers of the K $\alpha$  radiation of Cu (0.154252 nm), θ is the Bragg angle in radians, β (2θ) is the Full Width at Half Maximum (FWHM) of the diffraction peak in radians discounting instrumental contribution [FWHM(°) = 0.0755 + 4 × 10<sup>-4</sup>·2θ] and K is the shape factor constant, considered as 0.9.

The morphology of carbon supported nanoparticles was examined using a JEOL JSM-7000F scanning electron microscope (SEM) and a Philips CM200 transmission electron microscope (TEM) equipped with an EDXS collection unit. The samples for SEM were prepared just by deposition of the product on a carbon tape while those for TEM were dispersed on ethanol solution containing 5 %wt of *n*-decylamine and placed on a carbon-coated copper grid followed by drying under vacuum.

**X-ray structure determination.** Diffraction experiments were carried out on an Agilent Technologies SuperNova diffractometers (λ<sub>Cu-K $\alpha$</sub>  = 1.54184 Å for PdBPY, PdPHEN and CdNEO; λ<sub>Mo-K $\alpha$</sub>  = 0.71073 Å for ZnNEO, CdBPE and CdADE). Data were processed and corrected for Lorentz and polarization effects with the CrysAlisPro program.<sup>[25]</sup> The structures of all compounds were solved by direct methods using the SIR92 program (Table 4 and 5).<sup>[26]</sup> Full matrix least-squares refinements were performed on F<sup>2</sup> using SHELXL97.<sup>[27]</sup> All non-hydrogen atoms were refined anisotropically. All calculations for these structures were performed using the WINGX crystallographic software package.<sup>[28]</sup> During the data reduction process of PdPHEN, CdNEO and CdADE, it became clear that the crystal specimens were twinned with twin laws: (-0.9999 0.0002 -0.0000 / -0.0002 -1.0002 -0.0002 / 0.3008 -0.0007 0.9996) for PdPHEN; (-1.0000 -0.0005 0.0001 / 0.0159 0.0828 -0.9106 / -0.0160 -1.0899 -0.0850) for CdNEO; (-0.4089 0.0003 -0.5927 / -0.0003 -1.0000 -0.0001 / -1.4040 0.0010 0.4094) for CdADE. The final result showed a percentage for minor component of 45.9% (PdPHEN), 36.7% (CdNEO), 41.6% (CdADE). In compound CdBPE, one of the crystallographically independent thiobenzoate ligands is disordered over two almost coplanar arrangements with 50% occupation

factors. The internal carboxylate bond distances in the disordered thiocarboxylate were imposed to be nearly equal using SADI command.

Table 4. Crystal data and structure refinement of the compounds PdBPY, PdPHEN and ZnNEO.

Compound	PdBPY	PdPHEN	ZnNEO
Empirical formula	C <sub>24</sub> H <sub>18</sub> N <sub>2</sub> O <sub>2</sub> PdS <sub>2</sub>	C <sub>26</sub> H <sub>18</sub> N <sub>2</sub> O <sub>2</sub> PdS <sub>2</sub>	C <sub>28</sub> H <sub>22</sub> N <sub>2</sub> O <sub>2</sub> S <sub>2</sub> Zn
Mr [g mol <sup>-1</sup> ]	536.92	560.94	547.96
T [K]	100(2)	100(2)	293(2)
Crystal system	monoclinic	monoclinic	Orthorhombic
Space group	<i>C2/c</i> (No.15)	<i>I2/a</i> (No.15)	<i>Pbcn</i> (No.60)
a [Å]	23.9837(14)	10.1891(3)	20.8924(6)
b [Å]	9.4545(3)	10.4666(3)	13.3194(6)
c [Å]	9.8614(6)	20.3093(6)	9.1806(3)
α [°]	90	90	90
β [°]	112.358(7)	94.328(3)	90
γ [°]	90	90	90
V [Å <sup>3</sup> ]	2068.0(2)	2159.71(11)	2554.72(16)
Z	4	4	4
ρ <sub>calcd</sub> [g cm <sup>-3</sup> ]	1.725	1.725	1.425
μ [mm <sup>-1</sup> ]	9.335	8.972	1.153
F(000)	1080	1128	1128
θ range [°]	3.99–73.98	4.37–73.97	2.87–26.00
Reflections collected	2074	5464	2508
Independent reflections	2021	5159	1550
Parameters/restraints	141/0	151/0	160/0
R[I > 2σ(I)] <sup>[a]</sup>	R <sub>1</sub> = 0.0363 wR <sub>2</sub> = 0.1015	R <sub>1</sub> = 0.0428 wR <sub>2</sub> = 0.1190	R <sub>1</sub> = 0.0478 wR <sub>2</sub> = 0.1164
R (all data)	R <sub>1</sub> = 0.0370 wR <sub>2</sub> = 0.1019	R <sub>1</sub> = 0.0443 wR <sub>2</sub> = 0.1200	R <sub>1</sub> = 0.0802 wR <sub>2</sub> = 0.1317
GOF on F <sup>2</sup> (S) <sup>[b]</sup>	1.178	1.024	0.905
Weighting scheme <sup>[c]</sup>	SHELX	SHELX	SHELX

[a]  $R_1 = \sum(|F_o| - |F_c|)/\sum|F_o|$ ;  $wR_2 = \{\sum[w(F_o^2 - F_c^2)^2]/\sum[w|F_o|^2]\}^{1/2}$ . [b]  $S = [\sum w(|F_o| - |F_c|)^2/(N_{obs} - N_{param})]^{1/2}$ . [c] Scheme =  $I/[\sigma^2(F_o^2) + (aP)^2 + bP]$  where  $P = (F_o^2 + 2F_c^2)/3$ ; compound (a,b): PdBPY (0.0426, 16.6867), PdPHEN (0.1028, 0), and ZnNEO (0.0543, 0).

Table 5. Crystal data and structure refinement of the compounds CdBPE, CdNEO and CdADE.

Compound	CdBPE	CdNEO	CdADE
Empirical formula	C <sub>26</sub> H <sub>20</sub> CdN <sub>2</sub> O <sub>2</sub> S <sub>2</sub>	C <sub>28</sub> H <sub>22</sub> CdN <sub>2</sub> O <sub>2</sub> S <sub>2</sub>	C <sub>20</sub> H <sub>19</sub> CdN <sub>5</sub> O <sub>3</sub> S <sub>2</sub>
Mr [g mol <sup>-1</sup> ]	568.96	594.99	553.92
T [K]	100(2)	100(2)	100(2)
Crystal system	monoclinic	triclinic	monoclinic
Space group	<i>C2/c</i> (No.15)	<i>P</i> -1 (No.2)	<i>P2<sub>1</sub>/n</i> (No.14)
a [Å]	25.0653(5)	9.0970(7)	11.2499(5)
b [Å]	12.3273(2)	11.1808(10)	10.7383(5)
c [Å]	16.1337(3)	12.4222(9)	18.2771(7)
α [°]	90	81.599(7)	90
β [°]	105.714(2)	83.998(6)	96.992(4)
γ [°]	90	85.110(7)	90
V [Å <sup>3</sup> ]	4798.79(16)	1239.93(17)	2191.54(17)
Z	8	2	4
ρ <sub>calcd</sub> [g cm <sup>-3</sup> ]	1.575	1.594	1.679
μ [mm <sup>-1</sup> ]	1.110	8.859	1.219
F(000)	2288	600	1112
θ range [°]	1.69–28.30	3.61–74.00	2.02–28.35
Reflections collected	5488	8573	8763
Independent reflections	4917	6970	7085
Parameters/restraints	289/5	317/0	286/0
R[I > 2σ(I)] <sup>[a]</sup>	R <sub>1</sub> = 0.0425 wR <sub>2</sub> = 0.1000	R <sub>1</sub> = 0.0476 wR <sub>2</sub> = 0.1181	R <sub>1</sub> = 0.0285 wR <sub>2</sub> = 0.0718
R (all data)	R <sub>1</sub> = 0.0482 wR <sub>2</sub> = 0.1044	R <sub>1</sub> = 0.0578 wR <sub>2</sub> = 0.1214	R <sub>1</sub> = 0.0359 wR <sub>2</sub> = 0.0733
GOF on F <sup>2</sup> (S) <sup>[b]</sup>	1.039	0.959	0.975
Weighting scheme <sup>[c]</sup>	SHELX	SHELX	SHELX

[a]  $R_1 = \sum(|F_o| - |F_c|)/\sum|F_o|$ ;  $wR_2 = \{\sum[w(F_o^2 - F_c^2)^2]/\sum[w|F_o|^2]\}^{1/2}$ . [b]  $S = [\sum w(|F_o| - |F_c|)^2/(N_{obs} - N_{param})]^{1/2}$ . [c] Scheme =  $I/[\sigma^2(F_o^2) + (aP)^2 + bP]$  where  $P = (F_o^2 + 2F_c^2)/3$ ; compound (a,b): CdBPE (0.0390, 33.3626), CdNEO (0.0819, 0) and CdADE (0.0472, 0).

**Supporting Information** (see footnote on the first page of this article):  
Thermoanalytic data, PXRD patterns, FTIR spectra, SEM/TEM images, bond distances and angles, figures of crystal packings and thermolysis optimization experiments. Crystallographic data for structures reported in this paper have been deposited in the Cambridge Crystallographic Data Center under reference numbers CCDC 1552445-1552450. These data can be obtained free of charge via [www.ccdc.cam.ac.uk/data\\_request/cif](http://www.ccdc.cam.ac.uk/data_request/cif).

## Acknowledgments

This work has been funded by Universidad del País Vasco/Euskal Herriko Unibertsitatea (PPG17/37 and UFI 11/53) and Ministerio de Economía y Competitividad (MAT2016-75883-C2-1-P). Technical and human support

provided by SGIker (UPV/EHU, MICINN, GV/EJ, ESF) is also acknowledged.

## References

- [1] a) A. Kreider-Mueller, P. J. Quinlivan, J. S. Owen, G. Parkin, *Inorg. Chem.* **2015**, *54*, 3835–3850; b) S. Singh, S. Bhattacharya, *RSC Adv.* **2014**, *4*, 49491–49500; c) S. Singh, J. Chaturvedi, S. Bhattacharya, *Inorg. Chim. Acta* **2013**, *407*, 31–36; d) H. -Y. Chao, L. Wu, C. -L. Li, W. Lu, L. Liu, X. -L. Feng, *Z. Anorg. Allg. Chem.* **2011**, *637*, 1533–1538; e) M. El-khateeb, T. M. A. Jazzazi, H. Görls, T. M. A. Al-Shboul, M. Westerhausen, *Transition Met. Chem.* **2011**, *36*, 29–33; f) J. Chaturvedi, S. Singh, S. Bhattacharya, H. Nöth, *Inorg. Chem.* **2011**, *50*, 10056–10069; g) J. T. Sampanthar, J. J. Vittal, P. A. W. Dean, *J. Chem. Soc., Dalton Trans.* **1999**, 3153–3156.
- [2] a) J. Troyano, O. Castillo, P. Amo-Ochoa, V. Fernández-Moreira, C. J. Gómez-García, F. Zamora, S. Delgado, *J. Mater. Chem. C* **2016**, *4*, 8545–8551; b) B. M. Amoli, S. Gumfekar, A. Hu, Y. N. Zhou, B. Zhao, *J. Mater. Chem.* **2012**, *22*, 20048–20056; c) H. -Y. Chao, L. Wu, C. -L. Li, W. Lu, L. Liu, X. -L. Feng, *Z. Anorg. Allg. Chem.* **2011**, *637*, 1533–1538.
- [3] a) M. A. Buckingham, A. L. Catherall, M. S. Hill, A. L. Johnson, J. D. Parish, *Cryst. Growth Des.* **2017**, *17*, 907–912; b) D. C. Onwudiwe, C. A. Strydom, O. S. Oluwafemi, E. Hosten, A. Jordaan, *Dalton Trans.* **2014**, *43*, 8703–8712; c) S. L. Cumberland, K. M. Hanif, A. Javier, G. A. Khitrov, G. F. Strouse, S. M. Woessner, C. S. Yun, *Chem. Mater.* **2002**, *14*, 1576–1584; d) M. A. Malik, N. Revaprasadu, P. O'Brien, *Chem. Mater.* **2001**, *13*, 913–920.
- [4] a) X. Wang, G. Sun, N. Li, P. Chen, *Chem. Soc. Rev.* **2016**, *45*, 2239–2262; b) M. Kouhnavard, S. Ikeda, N. A. Ludin, N. B. A. Khairudin, B. V. Ghaffari, M. A. Mat-Teridi, M. A. Ibrahim, S. Sepeai, K. Sopian, *Renewable Sustainable Energy Rev.* **2014**, *37*, 397–407; c) C. Frigerio, D. S. M. Ribeiro, S. S. M. Rodrigues, V. L. R. G. Abreu, J. A. C. Barbosa, J. A. V. Prior, K. L. Marques, J. L. M. Santos, *Anal. Chim. Acta* **2012**, *735*, 9–22; d) T. -H. Kim, K. -S. Cho, E. K. Lee, S. J. Lee, J. Chae, J. W. Kim, D. H. Kim, J. -Y. Kwon, G. Amaratunga, S. Y. Lee, B. L. Choi, Y. Kuk, J. M. Kim, K. Kim, *Nat. Photonics* **2011**, *5*, 176–182; e) P. Xue, *Phys. Lett. A* **2010**, *374*, 2601–2604.
- [5] a) M. Hashemi, F. Mohandes, M. Salavati-Niasari, A. S. Esmaeily, *J. Mater. Sci.: Mater. Electron.* **2016**, *9*, 6860–6867; b) C. Zhang, S. Zhang, L. Yu, Z. Zhang, P. Zhang, Z. Wu, *Mater. Lett.* **2012**, *85*, 77–80; c) D. Jose, B. R. Jagirdar, *J. Solid State Chem.* **2010**, *183*, 2059–2067; d) H. G. Cha, D. K. Lee, Y. H. Kim, C. W. Kim, C. S. Lee, Y. S. Kang, *Inorg. Chem.* **2008**, *47*, 121–127.
- [6] a) S. H. Lu, T. F. Chen, A. J. Wang, D. Zheng, Y. L. Li, Y. S. Wang, *Mater. Sci. Eng., B* **2016**, *203*, 19–26; b) R. Gaur, P. Jeevanandam, *J. Nanopart. Res.* **2015**, *17*, 156–169; c) A. Ghezlbash, B. A. Korgel, *Langmuir* **2005**, *21*, 9451–9456.
- [7] a) A. Tiwari, A. K. Mishra, H. Kobayashi, A. P. F. Turner, *Intelligent Nanomaterials*, 1st ed., Wiley, New Jersey, **2012**, pp. 251–316; b) H. S. Park, S. D. Waezsada, A. H. Cowley, H. W. Roesky, *Chem. Mater.* **1998**, *10*, 2251–2257.
- [8] a) X. Du, H. Zhao, Z. Zhang, Y. Lu, C. Gao, Z. Li, Y. Teng, L. Zhao, K. Swierczek, *Electrochim. Acta* **2017**, *225*, 129–136; b) J. Chen, F. Zhang, Y. -L. Zhao, Y. -C. Guo, P. Gong, Z. -Q. Li, H. -S. Qian, *Appl. Surf. Sci.* **2016**, *362*, 126–131; c) B. K. Barman, K. K. Nanda, *Dalton Trans.* **2016**, *45*, 6352–6356; d) Y. Hu, X. Gao, L. Yu, Y. Wang, J. Ning, S. Xu, X. W. Lou, *Angew. Chem. Int. Ed.* **2013**, *52*, 5636–5639; e) H. Ma, J. Han, Y. Fu, Y. Song, C. Yu, X. Dong, *Appl. Catal., B* **2011**, *102*, 417–423.
- [9] a) D. Duan, X. You, J. Liang, S. Liu, Y. Wang, *Electrochim. Acta* **2015**, *176*, 1126–1135; b) A. Sáez, J. Solla-Gullón, E. Expósito, A. Aldaz, V. Montiel, *Int. J. Electrochem. Sci.* **2013**, *8*, 7030–7043; c) G. F. Álvarez, M. Mamlouk, S. M. S. Kumar, K. Scott, *J. Appl. Electrochem.* **2011**, *41*, 925–937; d) S. Rojas, F. J. García-García, S. Járas, M. V. Martínez-Huerta, J. L. G. Fierro, M. Boutonnet, *Appl. Catal., A* **2005**, *285*, 24–35.
- [10] a) A. Zahoor, M. Christy, Y. Kim, A. Arul, Y. S. Lee, K. S. Nahm, *J. Solid State Electrochem.* **2016**, *20*, 1397–1404; b) R. D. McKerracher, C. Alegre, V. Baglio, A. S. Arico, C. Ponce de León, E. Mornaghini, M. Rodlert, F. C. Walsh, *Electrochim. Acta* **2015**, *174*, 508–515; c) F. Li, Y. Chen, D. -M. Tang, Z. Jian, C. Liu, D. Golberg, A. Yamada, H. Zhou, *Energy Environ. Sci.* **2014**, *7*, 1648–1652.
- [11] a) K. D. Collins, R. Honeker, S. Vázquez-Céspedes, D. -T. D. Tang, F. Glorius, *Chem. Sci.* **2015**, *6*, 1816–1824; b) S. Hayashi, Y. Kojima, T. Koizumi, *Polym. Chem.* **2015**, *6*, 881–885; c) F. -X. Felpin, T. Ayad, S. Mitra, *Eur. J. Org. Chem.* **2006**, 2679–2690; d) A. Perosa, P. Tundo, M. Selva, S. Zinovyev, A. Testa, *Org. Biomol. Chem.* **2004**, *2*, 2249–2252; e) N. Nakamichi, Y. Kawashita, M. Hayashi, *Org. Lett.* **2002**, *4*, 3955–3957.
- [12] a) F. Cui, G. Li, X. Li, M. Lu, M. Li, *Catal. Sci. Technol.* **2015**, *5*, 549–555; b) E. J. M. Hensen, H. J. A. Brans, G. M. H. J. Lardinois, V. H. J. De Beer, J. A. R. Van Veen, R. A. Van Santen, *J. Catal. Technol.* **1989**, *2*, 107–133.
- [13] a) S. Karthikeyan, R. Boopathy, G. Sekaran, *J. Colloid Interface Sci.* **2015**, *448*, 163–174; b) A. Rodríguez, G. Ovejero, M. D. Romero, C. Díaz, M. Barreiro, J. García, *J. Supercrit. Fluids* **2008**, *46*, 163–172; c) S. Cao, G. Chen, X. Hu, P. L. Yue, *Catal. Today* **2003**, *88*, 37–47.
- [14] a) M. Sterrer, H. -J. Freund, *Catal. Lett.* **2013**, *143*, 375–385; b) X. Liu, J. G. Khinast, B. J. Glasser, *Chem. Eng. Sci.* **2008**, *63*, 4517–4530; c) G. Li, L. Hu, J. M. Hill, *Appl. Catal., A* **2006**, *301*, 16–24; d) A. J. Van Dillen, R. J. A. M. Terörde, D. J. Lensveld, J. W. Geus, K. P. De Jong, *J. Catal.* **2003**, *216*, 257–264; e) M. Campanati, G. Fornasari, A. Vaccari, *Catal. Today* **2003**, *77*, 299–314.
- [15] D. Vallejo-Sánchez, G. Beobide, O. Castillo, M. Lanchas, *Eur. J. Inorg. Chem.* **2013**, 5592–5602.
- [16] a) M. Pinsky, D. Avnir, *Inorg. Chem.* **1998**, *37*, 5575–5582. b) D. Casanova, J. Cirera, M. Llunell, P. Alemany, D. Avnir, S. Alvarez, *J. Am. Chem. Soc.* **2004**, *126*, 1755–1763.
- [17] a) <http://sdfs.db.aist.go.jp>; b) <http://webbook.nist.gov/chemistry/> (last accessed on 2017/12/17).
- [18] a) B. R. Stanmore, J. F. Brilhac, P. Gilot, *Carbon* **2001**, *39*, 2247–2268; b) I. M. Kennedy, *Prog. Energy Combust. Sci.* **1997**, *23*, 95–132.
- [19] a) H. F. M. Dacosta, J. J. Driscoll, T. E. Paulson, W. J. Robel, S. M. Zemskova, US2009056320-A1; b) H. S. Han, J. H. Bae, KR2007005406-A.
- [20] F. A. La Porta, J. Andrés, M. S. Li, J. R. Sambrano, J. A. Varela, E. Longo, *Phys. Chem. Chem. Phys.* **2014**, *16*, 20127–20137.
- [21] a) S. Biswas, S. Kar, *Nanotechnology* **2008**, *19*, 045710; b) H. Zhang, L. Qi, *Nanotechnology* **2006**, *17*, 3984–3988.
- [22] a) C. Suryanarayana, M. G. Norton, *X-Ray Diffraction, A Practical Approach*, Plenum Press, New York, **1998**, pp. 207–221; b) J. I. Langford, A. J. C. Wilson, *J. Appl. Cryst.* **1978**, *11*, 102–113; c) P. Scherrer, *Nachr. Ges. Wiss. Göttingen* **1918**, *26*, 98–100.
- [23] a) S. Muruganandam, G. Anbalagan, G. Murugadoss, *Optik* **2017**, *131*, 826–837; b) G. B. Shombe, E. B. Mubofu, S. Mlowe, N. Revaprasadu, *Mater. Sci. Semicond. Process* **2016**, *43*, 230–237; c) V. Singh, P. Chauhan, *J. Phys. Chem. Solids* **2009**, *70*, 1074–1079.
- [24] a) S. K. Maji, N. Mukherjee, A. Mondal, B. Adhikary, B. Karmakar, S. Dutta, *Inorg. Chim. Acta* **2011**, *371*, 20–26; b) T. C. Deivaraj, J. -H. Park, M. Afzaal, P. O'Brien, J. J. Vittal, *Chem. Mater.* **2003**, *15*, 2383–2391.
- [25] *CrysAlisPro*, version 1.171.35.15; Agilent Technologies: Yarnton, U. K., **2011**.
- [26] A. Altomare, M. Cascarano, C. Giacovazzo, A. Guagliardi, *J. Appl. Crystallogr.* **1993**, *26*, 343–350.
- [27] G. M. Sheldrick, *Acta Crystallogr., Sect. A: Found. Crystallogr.* **2008**, *A64*, 112–122.
- [28] L. J. Farrugia, *J. Appl. Crystallogr.* **1999**, *32*, 837–838.

Received: ((will be filled in by the editorial staff))  
Published online: ((will be filled in by the editorial staff))

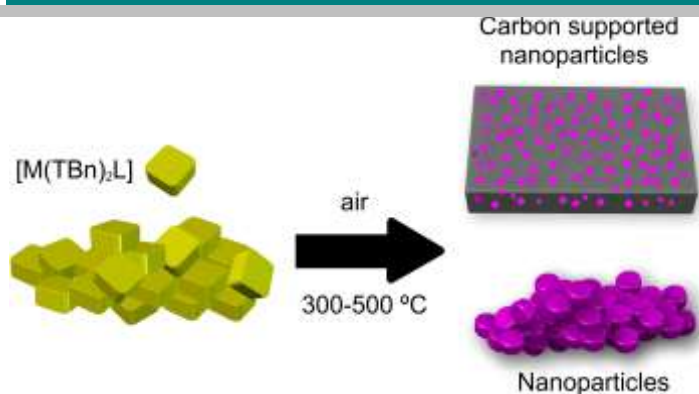
Received: ((will be filled in by the editorial staff))  
Published online: ((will be filled in by the editorial staff))

Accepted Manuscript



## Entry for the Table of Contents

## FULL PAPER



Six new air-stable metal-thiobenzoato compounds with *N*-heterocycles have been synthesized and structurally characterized. Their solventless thermolysis under aerobic conditions and at relatively mild temperature (350–480°C) provides in a single step carbon supported metal and metal sulfide nanoparticles with high crystallinity.

**Dry-thermolysis / Carbon supported nanoparticles \***

*Daniel Vallejo-Sánchez, Garikoitz Beobide,\* Oscar Castillo,\* Mónica Lanchas, Antonio Luque, Sonia Pérez-Yáñez, Pascual Román*

**Page No. – Page No.**

**Metal-thiobenzoato complexes: synthesis, structure and processing as carbon supported nanoparticles**

Accepted Manuscript